Polymer 185 (2019) 121940

Contents lists available at ScienceDirect

Polymer

journal homepage: http://www.elsevier.com/locate/polymer

Highly thermally stable mesoporous Poly(cyanate ester) featuring double-decker–shaped polyhedral silsesquioxane framework

Wei-Cheng Chen [a], Mahmoud M.M. Ahmed [a], Chih-Feng Wang [b], Chih-Feng Huang [c], Shiao-Wei Kuo [a,d,*]

[a] Department of Materials and Optoelectronic Science, Center of Crystal Research, National Sun Yat-Sen University, Kaohsiung, 80424, Taiwan
[b] Advanced Membrane Materials Research Center, Graduate Institute of Applied Science and Technology, National Taiwan University of Science and Technology, Taipei, 10607, Taiwan
[c] Department of Chemical Engineering, National Chung Hsing University, 145 Xingda Road, Taichung, 402-27, Taiwan
[d] Department of Medicinal and Applied Chemistry, Kaohsiung Medical University, Kaohsiung, 807, Taiwan

ARTICLE INFO

Keywords:
Poly(cyanate ester)
DDSQ
Nanocomposites

ABSTRACT

In this study we prepared cyanate ester–functionalized double-decker silsesquioxane (DDSQ) nanoparticles through a sequence of hydrosilylation of nadic anhydride (ND) with DDSQ and then treat with 4-aminophenol to provide DDSQ-ND-OH, and reaction with cyanogen bromide (BrCN) to form DDSQ-ND-OCN (a bis-phenyl cyanate ester DDSQ). After thermal curing of DDSQ-ND-OCN, we obtained mesoporous poly(cyanate ester) (PCE)/DDSQ frameworks that displayed high thermal stabilities and char yields since the inorganic DDSQ nanoparticles were dispersed in the PCE matrix homogeneously, as revealed using electron microscopy. Thermal polymerization at 210 °C provided a PCE/DDSQ framework having a thermal decomposition temperature (516 °C) and char yield (70 wt%); these values increased to 600 °C and 81 wt%, respectively, after thermal treatment at 420 °C. More interestingly, these mesoporous PCE/DDSQ frameworks displayed electrochemical properties better than those of other non-carbonized materials.

1. Introduction

Polycyanates are used widely in high-performance and functional materials, including composite resin substrates and digital printed circuit boards, because of their low dielectric constants, excellent heat resistance, low moisture absorption, and volume shrinkage [1–3]. A large number of commercially available cyanate resins are bisphenol A–type cyanate resins, because their industrial synthesis is simple and their raw materials are available cheaply. The main disadvantage of such dicyanate resins is that they become brittle after thermal hardening [4,5]. First stable aromatic dicyanate was synthesized by Gripat et al. from a phenol and a cyanogen halide [1]. Several related products have been proposed for real industrial applications. Polycyanate resins can be prepared through heat-curing of dicyanate monomers; the hardening reaction occurs mainly through polycyclotrimerization to form a cross-network structure. The pure cyanate does not react when heated. Bauer et al. suggested that the cyanate reactant must contain a small amount of residual phenol or water as a residual impurity that can catalyze the cyclization reaction [6]. Gupta and Macosko heated a monofunctional 2-(4-cyanatophenyl)-2-phenylpropane to obtain a para-form product; polycondensation was presumably the main reaction that led to the formation of an s-triazine in a yield of greater than 90% [7].

A typical type of poly(cyanate ester) (PCE) is that synthesized from bisphenol A and cyanogen bromide; this material displays the thermal decomposition temperature (T_d) of 411 °C and the char yield of 41 wt%.[1] Many approaches have been examined to improve the physical properties of PCEs for example, introducing reactive functional groups into the cyanate ester monomers [8–10] and mixing inorganic nanoparticles [e.g., polyhedral oligomeric silsesquioxane (POSS), carbon nanotubes, clay, graphene] into the PCE matrix [11–16]. In general, the incorporation of POSS into a polymer improves the thermal stability, increases the oxidation resistance, decreases the flammability, and lowers the surface free energy [17–23]. The inorganic POSS nanoparticles in such polymer/POSS hybrids can be positioned at the side chains or chain ends through reactions of mono-functionalized POSS compounds [24–30].

* Corresponding author. Department of Materials and Optoelectronic Science, Center of Crystal Research, National Sun Yat-Sen University, Kaohsiung, 80424, Taiwan.
E-mail address: kuosw@faculty.nsysu.edu.tw (S.-W. Kuo).

https://doi.org/10.1016/j.polymer.2019.121940
Received 14 August 2019; Received in revised form 19 October 2019; Accepted 23 October 2019
Available online 26 October 2019

Insoluble cross-linked polymers have been obtained when reacting multi-functionalized POSS compounds (with greater than two functional units) [31–33]. Furthermore, bifunctionalized POSS derivatives including double-decker–shaped polyhedral silsesquioxanes (DDSQs) have been developed to produce new main chain type polymer/POSS nanocomposites for polyurethane, polyimide, and polybenzoxazine matrices [34–41]. Because DDSQs possess hollow and bulky structures, they can increase the free volume of a polymer and lower its dielectric constant [34–41]. Furthermore, because they are highly thermally stable, it is expected that introducing inorganic DDSQ cage structures (through covalent bonding or dispersion) should enhance the thermal properties of conventional PCE matrices.

In this study, we introduced DDSQ nanoparticles into a PCE matrix to form a new organic/inorganic hybrid (Scheme 1). We first synthesized a bifunctional phenolic DDSQ derivative [Scheme 1(a)–(e)] and then formed a bifunctional cyanate ester DDSQ (DDSQ-ND-OCN) through a reaction with cyanogen bromide (BrCN) [Scheme 1(f)]. Mesoporous PCE/DDSQ frameworks were obtained after thermal curing, where ring cyclotrimerization of the OCN units created a high concentration of s-triazine rings linked through ether units to the benzene rings of the bisphenol DDSQ (Scheme 2). The chemical structure of the monomer DDSQ-ND-OCN was confirmed by Fourier transform infrared (FTIR) spectroscopy, NMR spectroscopy, and mass-analyzed laser desorption/ionization time-of-flight (MALDI-TOF) mass spectrometry.

2. Experimental section

2.1. Materials

Phenyltrimethoxysilane, platinum divinyltetramethyldisiloxane complex [Pt(dvs)], methyl dichlorosilane, 2-propanol, tetrahydrofuran (THF), sodium hydroxide (NaOH), charcoal, and magnesium sulfate ($MgSO_4$) were purchased from Alfa–Aesar. Nadic anhydride (ND), 4-aminophenol, cyanogen bromide (BrCN), ethanol (EtOH), methanol (MeOH), sodium bicarbonate ($NaHCO_3$), acetonitrile, and cyclohexane were purchased from Sigma–Aldrich. DDSQ-ND-OH was synthesized as described previously [Scheme 1(e)] [34,35].

2.2. Synthesis and thermal curing of the bisphenyl cyanate ester double-decker silsesquioxane (DDSQ-ND-OCN)

DDSQ-ND-OH (4.5 g, 2.7 mmol) and BrCN (0.85 g, 8.1 mmol) were

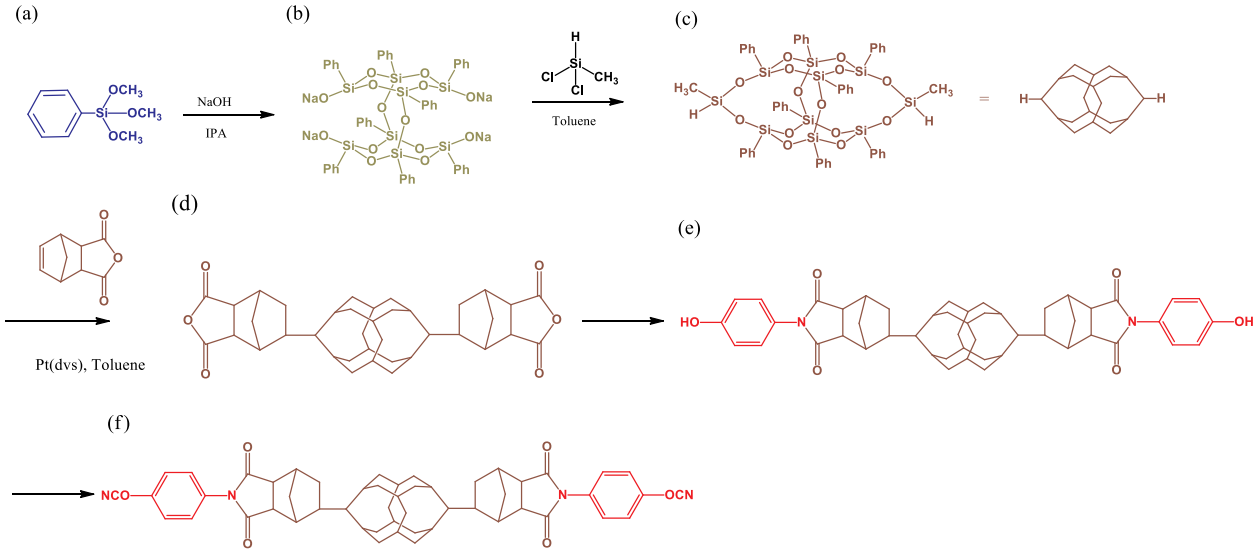

Scheme 1. Synthesis of the monomer DDSQ-ND-OCN (f) from (a) phenyltrimethoxysilane, (b) DD-Na, (c) DDSQ, (d) DDSQ-ND, and (e) DDSQ-ND-OH.

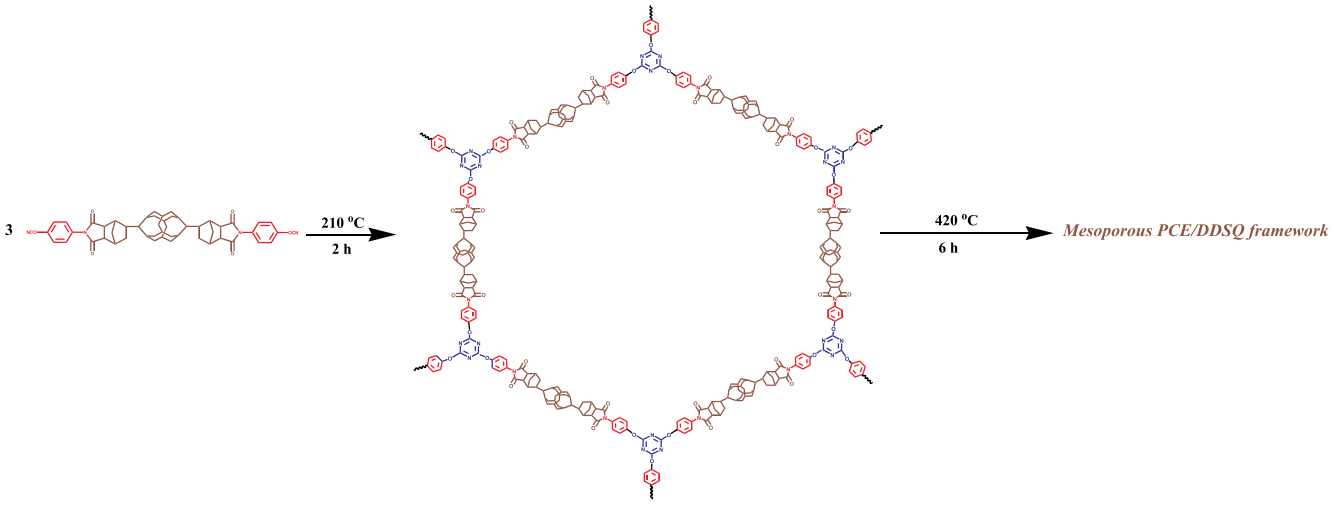

Scheme 2. (a) Chemical structure of DDSQ-ND-OCN; (b) thermal trimerization of DDSQ-ND-OCN at 210 °C for 2 h; (c) mesoporous PCE/DDSQ framework after thermal treatment at 420 °C for 6 h.

placed under a blanket of N_2. THF (20 mL) was added dropwise while stirring vigorously. The solution was cooled to −30 °C and then triethylamine (0.42 mL) was added dropwise over 30 min. The temperature was maintained at −20 °C by immersion in a Dewar flask containing a MeOH/liquid N_2 mixture. The reaction was complete after 4 h. The white salt was filtered off. Ice water (500 mL) was added to the filtrate to give a red precipitate. This crude product was recrystallized (cyclohexane) to give a pink powder (3.69 g, yield: 82%). The DDSQ-ND-OCN monomer was placed in the aluminum pan and then subjected to thermal curing for 2 h at various temperatures (90, 150, 180, and 210 °C) to give PCE/DDSQ hybrid. Then, the PCE/DDSQ hybrid was subjected to thermal treatment at 420 °C for 6 h to afford mesoporous PCE/DDSQ framework (3.00 g, yield: 82%).

3. Results and discussion

3.1. Synthesis of the DDSQ-functionalized benzoxazine monomer

Scheme 1 shows the synthesis of the DDSQ-ND-OCN monomer. The chemical structure of each intermediate was confirmed by MALDI-TOF mass spectrometry and ^{1}H NMR and FTIR spectroscopy. Fig. 1 provides FTIR spectra of each compound obtained during the preparation of the monomer DDSQ-ND-OCN. The spectrum of each DDSQ compound featured a strong signal for the Si–O–Si units at 1097 cm^{-1} and a weak signal at 1261 cm^{-1} for the $SiCH_3$ units. Furthermore, a signal at 2172 cm^{-1}, representing Si–H stretching, appeared for pure DDSQ [Fig. 1(a)], but it disappeared after the hydrosilylation of ND with DDSQ. Fig. 1(b) reveals that two new signals appeared at 1782 and 1860 cm^{-1}, representing the anhydride C═O groups of DDSQ-ND, confirming the success of the hydrosilylation. The DDSQ-ND-OH spectrum [Fig. 1(c)] reveals signals for the C═O imide units at 1700 and 1771 cm^{-1}, a broad signal centered at 3395 cm^{-1} for the OH units, and a signal at 1390 cm^{-1} for the CN units; these shifts to lower wavenumbers for the signals of the C═O and OH units are consistent with the DDSQ-ND-OH formation [35]. Fig. 1(d) reveals that the signals for imide C═O absorption had red-shifted to 1709 and 1772 cm^{-1} and that signals for OCN units appeared at 2277, 2239, and 2201 cm^{-1} [4,42], confirming the formation of the monomer DDSQ-ND-OCN.

Fig. 2 presents ^{1}H and ^{13}C NMR spectra of DDSQ-ND-OH and DDSQ-ND-OCN. ^{1}H NMR spectrum of DDSQ-ND-OH [Fig. 2(a)] features the aromatic proton signals of the 4-aminophenol units at 6.80 (*k*) and 6.24 (*l*) ppm (Scheme S1) and a broad signal near 5.33 ppm for the OH units [35]. This signal for the phenolic OH protons was disappeared by ^{1}H NMR spectrum of the monomer DDSQ-ND-OCN [Fig. 2(b)]. Similarly, the ^{13}C NMR spectrum of DDSQ-ND-OH features a signal at 156.9 ppm for *$\mathbf{C}_{AR}$-OH units [Fig. 2(c)]; this signal shifted to 152.7 ppm for the *$\mathbf{C}_{AR}$-OCN units, while a new signal appeared at 108.8 ppm for the O*$\mathbf{C}$N units, in the ^{13}C NMR spectrum of DDSQ-ND-OCN [Fig. 2(d)]. Fig. S1 displays the MALDI-TOF mass spectrum of DDSQ-ND-OCN, with its molecular ion located at *m/z* 1737, consistent with the structure of this DDSQ derivative. Thus, the FTIR, NMR, and mass spectra confirmed the synthesis of the monomer DDSQ-ND-OCN.

3.2. Thermal curing behavior of the monomer DDSQ-ND-OCN

We used DSC to examine the thermal polymerization of the monomer DDSQ-ND-OCN. Fig. 3(A) displays DSC thermograms of the monomer DDSQ-ND-OCN after applying each thermal polymerization procedure. The uncured monomer DDSQ-ND-OCN provided the thermal curing exothermic peak at 205 °C and the reaction heat of 33.4 J/g [Fig. 3(A)–(a)]. This reaction heat of DDSQ-ND-OCN was decreased with the increase of the thermal curing temperature (Fig. S2). This exothermic peak was totally disappeared as the thermal curing temperature was higher than 210 °C [Fig. 3(A)–(e)], suggesting that the thermal polymerization temperature of DDSQ-ND-OCN was greater than 210 °C. The thermal polymerization behavior of DDSQ-ND-OCN was confirmed through FTIR

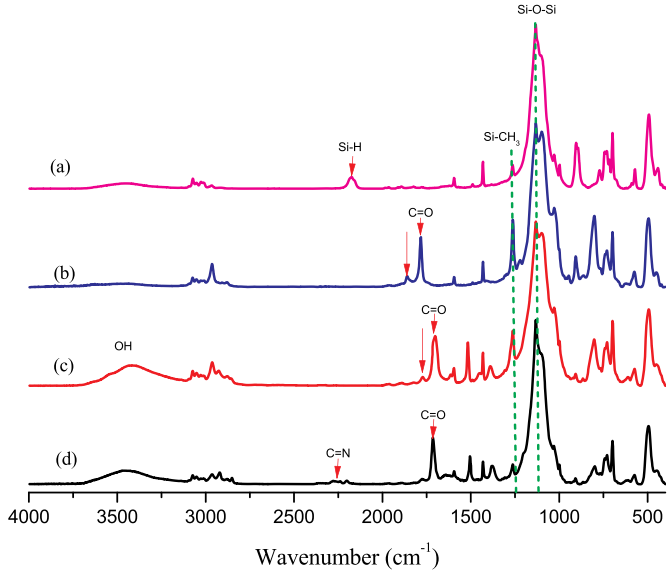

Fig. 1. FTIR spectra recorded at room temperature of (a) DDSQ, (b) DDSQ-ND, (c) DDSQ-ND-OH, and (d) the monomer DDSQ-ND-OCN.

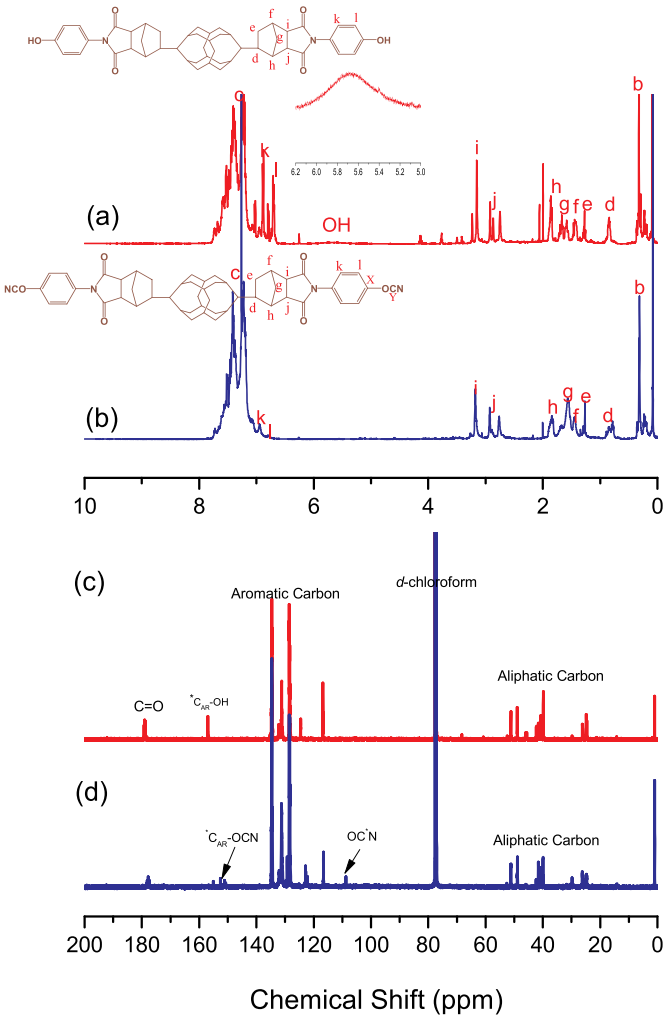

Fig. 2. (a, b) ^{1}H and (c, d) ^{13}C NMR spectra of (a, c) DDSQ-ND-OH and (b, d) the monomer DDSQ-ND-OCN.

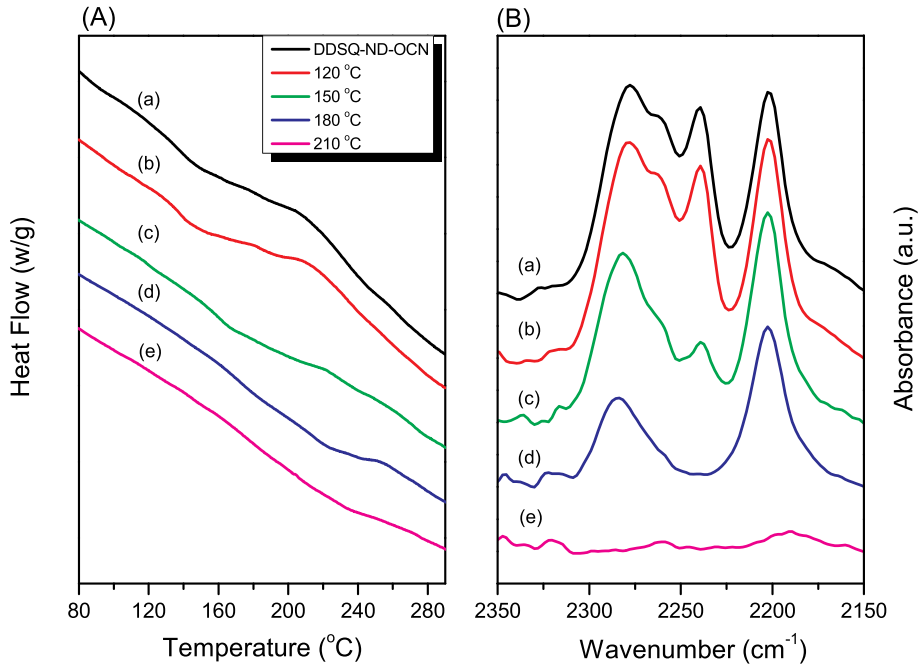

Fig. 3. (A) DSC traces, recorded at heating rate of 20 °C/min with a heat flow (50 mL/min) and (B) FTIR spectra of the monomer DDSQ-ND-OCN: (a) uncured and (b)–(e) measured after curing at for 2 h at various temperatures of (b) 120, (c) 150, (d) 180, and (e) 210 °C.

spectral analyses [Fig. 3(B)]. These intensities of the characteristic absorption peaks of the uncured DDSQ-ND-OCN at 2277, 2239, and 2201 cm^{-1} decreased gradually with the increase of thermal polymerization temperature and completely disappeared as the thermal polymerization temperature was 210 °C [Fig. 3(B)–(e)]. This behavior is consistent with the OCN groups forming triazine units after thermal curing at 210 °C to obtain a highly crosslinked PCE/DDSQ hybrid, without the need for a catalyst.

Fig. 4 displays the corresponding TGA spectra of DDSQ-ND-OCN after each thermal curing process. The value of T_d (10 wt% loss) and the char yield of the monomer DDSQ-ND-OCN were 515 °C and 68 wt%, respectively, confirming its high thermal stability. After thermal curing at 210 °C, the value of T_d and the char yield increased to 526 °C and 72 wt%, respectively, because the formation of triazine units increased the crosslinking density [Scheme 2(b)]; these two values increased significantly to 600 °C and 81 wt%, respectively, after thermal treatment at 420 °C, due to the formation of a mesoporous PCE/DDSQ framework having a hexagonal structure [Scheme 2(c)].

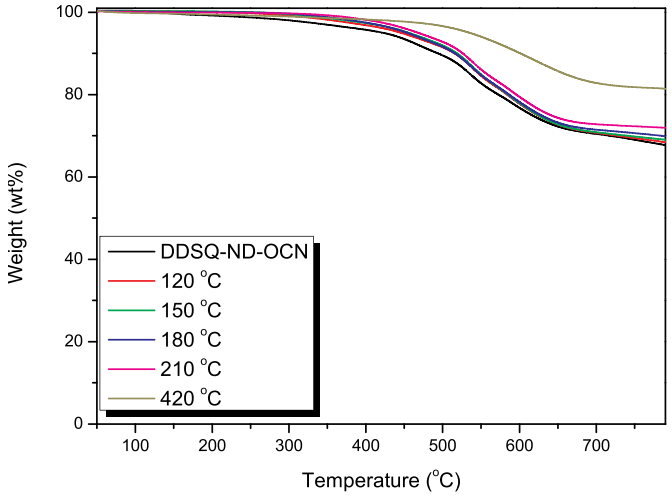

Fig. 4. TGA traces of the monomer DDSQ-ND-OCN, recorded after each curing stage.

Nevertheless, although the latter value of T_d was 600 °C, the onset temperature for thermal degradation of that mesoporous PCE/DDSQ framework was approximately 500 °C. We recorded N_2 isotherm sorption curves to examine the surface areas and pore sizes of the mesoporous PCE/DDSQ frameworks obtained after thermal treatment at 420 and 500 °C [Fig. 5(a)]. A typical type-IV with H_1 type of hysteresis loop appeared for the mesoporous PCE/DDSQ framework after thermal treatment at 420 °C, suggesting the presence of cylindrical pores. The pore size and surface area of this mesoporous PCE/DDSQ framework, measured using the BJH method, was greater than 2 nm (average pore size: 5.6 nm) and 392 $m^2 g^{-1}$, respectively [Fig. 5(b)]. In contrast, the sorption/desorption curve collapsed and, thus, the surface area decreased to 235 $m^2 g^{-1}$ and the pore size distribution could not be determined for the mesoporous PCE/DDSQ framework after thermal treatment at 500 °C, implying that the hexagonal porous framework structure may have collapsed at this temperature.

We used XRD, SEM, TEM, FTIR spectroscopy, and solid state NMR spectroscopy to examine the change in chemical structure of the mesoporous PCE/DDSQ framework after thermal treatment at 420 and 500 °C. Fig. 6(a) displays the XRD pattern of the mesoporous PCE/DDSQ framework after thermal treatment at 420 °C; the peak position ratio of the values of q were $1:\sqrt{3}:2:\sqrt{7}$, indicative of a hexagonally packed cylindrical structure and consistent with the apparent micropores in TEM images in Fig. 6(b) and (c). The first value of q was located at 0.4 A^{-1}, corresponding to a d-spacing of 1.57 nm, based on the Bragg equation. Fig. 6(b) also reveals a highly ordered lamellar or layer structure for the mesoporous PCE/DDSQ framework. We observed no discernible phase separation and a featureless morphology in the SEM image of the mesoporous PCE/DDSQ framework [Fig. 6(d)], suggesting that the inorganic DDSQ units had dispersed homogeneously in the PCE matrix. Fig. 6(e)–(h) display the energy-dispersive X-ray (EDX) Si, C, and N spectroscopic mappings of the mesoporous PCE/DDSQ framework; they also suggest that inorganic DDSQ units were dispersed well in PCE matrix. For example, Fig. 6(e) displays a red point, representing a DDSQ-enriched region, that suggests no aggregation of spherical nanoparticles, thereby confirming that DDSQ nanoparticles were dispersed well in PCE matrix.

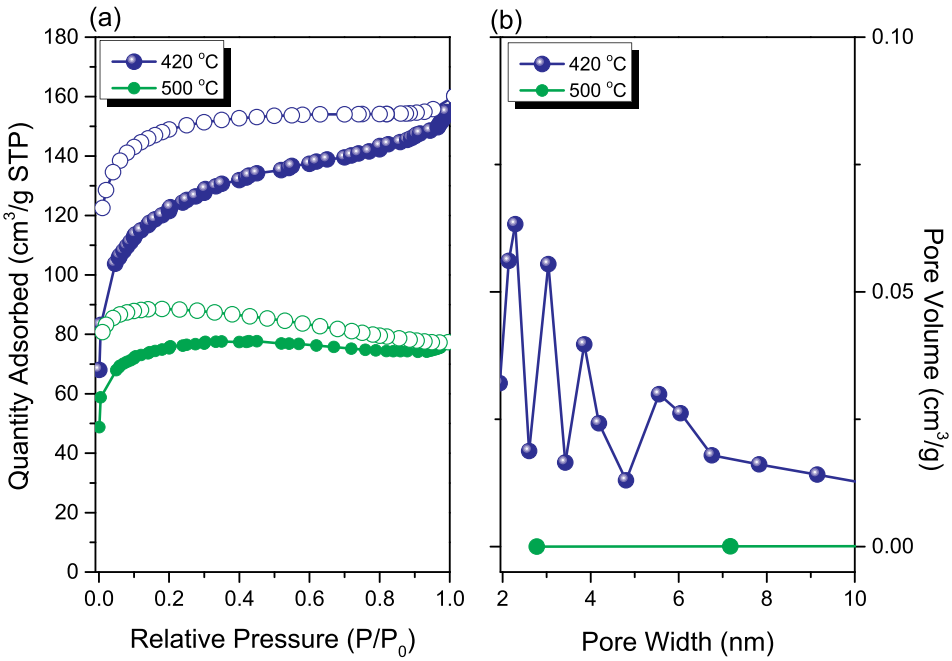

Fig. 5. (a) N_2 adsorption/desorption isotherms (adsorption (●, filled cycles) and desorption (○, open cycles) and (b) pore size distributions of DDSQ-ND-OCN after thermal treatment at 420 and 500 °C.

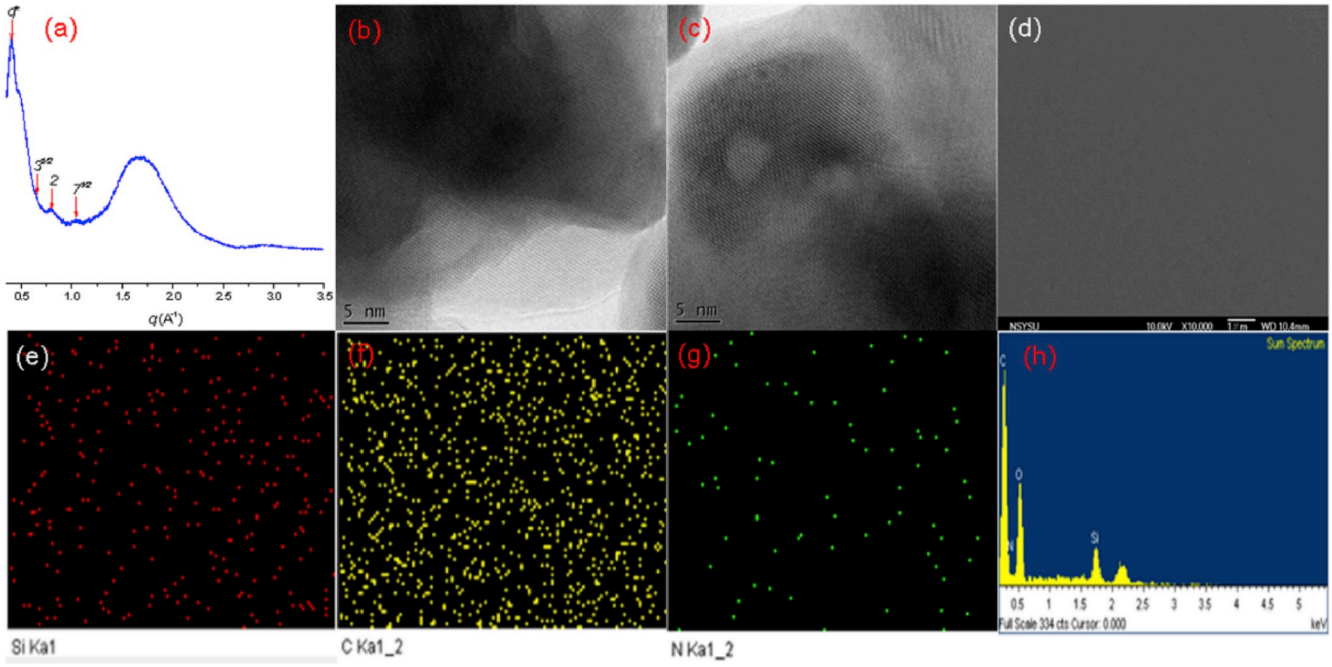

Fig. 6. (a) XRD; (b, c) TEM; (d) SEM; (e) Si, (f) C, and (g) N mapping; and (h) EDX analyses of the monomer DDSQ-ND-OCN after thermal treatment at 420 °C.

Furthermore, Fig. 7(a) presents the corresponding XRD pattern of the mesoporous PCE/DDSQ framework after thermal treatment at 500 °C; the peak ratio of 1:2:$\sqrt{7}$ also suggests a hexagonally packed cylindrical structure, consistent with the TEM images in Fig. 7(b) and (c). Similarly, Fig. 7(c) also suggests a highly ordered layer structure for the mesoporous PCE/DDSQ framework after thermal treatment at 500 °C. No obvious phase separation and a featureless morphology appear in the SEM image of the mesoporous PCE/DDSQ framework after thermal treatment at 500 °C [Fig. 7(d)]. Furthermore, the EDX spectral Si, C, and N mappings of the mesoporous PCE/DDSQ framework [Fig. 6(e)–(h)] after thermal treatment at 500 °C also imply that the inorganic DDSQ units were also dispersed homogeneously. We found, however, that the Si concentration increased significantly from 9.97 to 16.23 wt% and the C concentration decreased significantly from 42.15 to 36.08 wt% after thermal treatment of the mesoporous PCE/DDSQ framework at 500 °C, when compared with the sample obtained after thermal treatment at 420 °C [cf. Figs. 6(h) and 7(h)].

Taking into account the chemical structure of the mesoporous PCE/DDSQ framework, we suspect that the aliphatic CH_2 units of the ND groups may have possessed relatively lower thermal stability, such that the hexagonally packed cylindrical porous structure may have collapsed as a result of cleavage of some of the C–H or C═O bonds of the ND

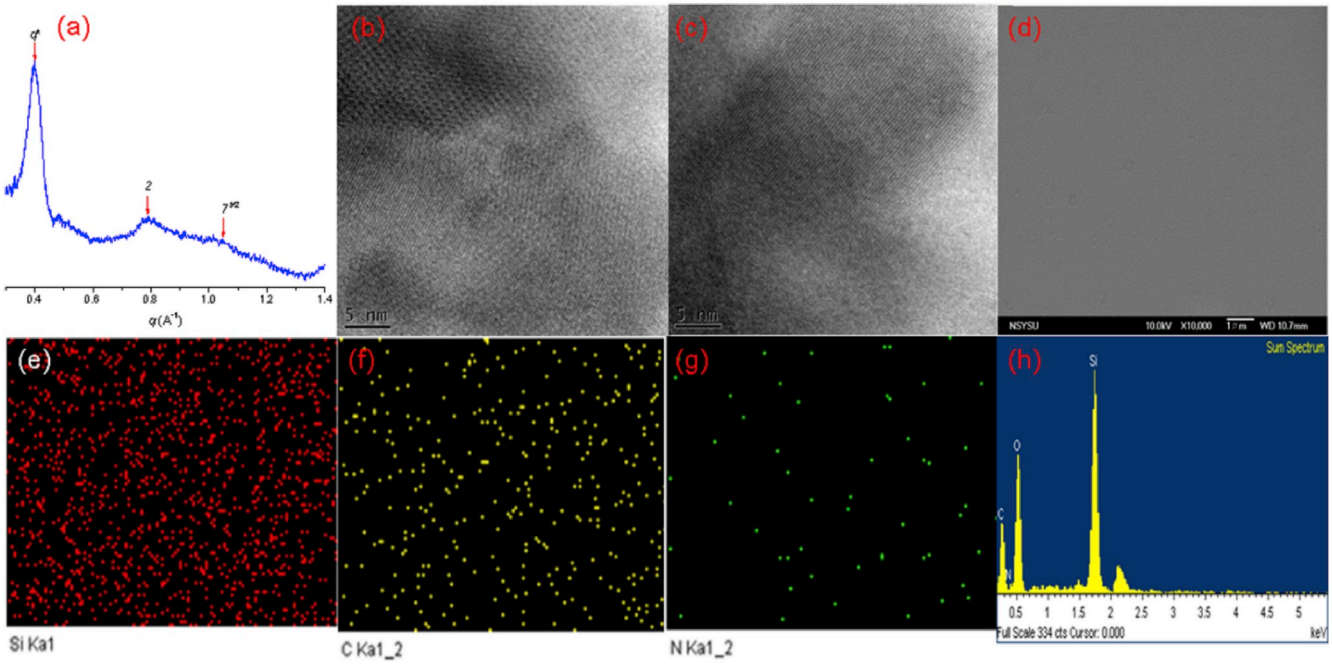

Fig. 7. (a) XRD; (b, c) TEM; (d) SEM; (e) Si, (f) C, and (g) N mapping; and (h) EDX analyses of the monomer DDSQ-ND-OCN after thermal treatment at 500 °C.

groups (Scheme S2). We used FTIR spectroscopy and ^{13}C and ^{29}Si solid state NMR spectroscopy to investigate the change in the chemical structure after thermal treatment at each temperature. Fig. 8(a) presents FTIR spectra of the monomer DDSQ-ND-OCN after its thermal treatment at various temperatures. The signals for Si–O–Si stretching (at 1089 and 1130 cm^{-1}) and Si–CH_3 stretching (at 1261 cm^{-1}) did not change after treatment at the various temperatures, suggesting that the inorganic DDSQ nanoparticles were not destroyed under high-temperature thermal treatment. New signals for C═N absorption appeared at 1653 and 1563 cm^{-1} [43] consistent with the formation of triazine units and the disappearance of the signals for the OCN units in Fig. 3(B). As thermal treatment temperature was 420 °C, the FTIR spectrum remained almost unchanged relative to room temperature, indicating that the chemical structure did not change appreciably; in contrast, the intensity of the

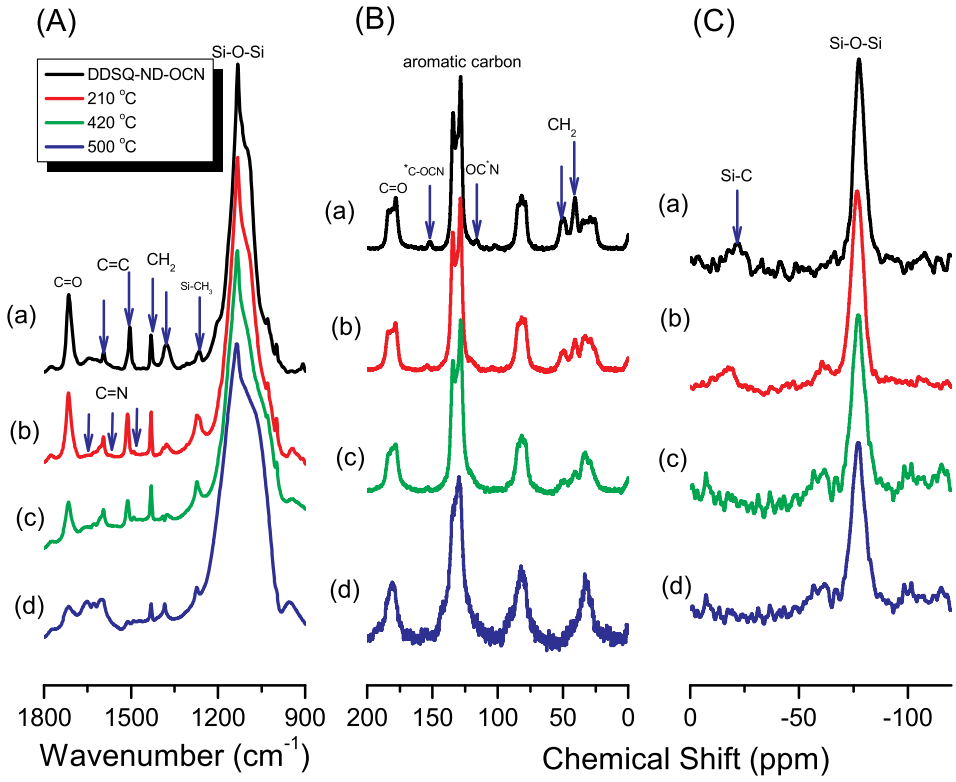

Fig. 8. (A) FTIR spectra and (B) ^{13}C and (C) ^{29}Si solid state NMR spectra of DDSQ-ND-OCN: (a) uncured and (b)–(d) recorded after thermal treatment at (b) 210, (c) 420, and (d) 500 °C.

signals for the aliphatic CH_2 units at 1433 cm^{-1} and the C═O units at 1709 cm^{-1} from the ND moieties both decreased after thermal treatment at 500 °C. Fig. 8(b) presents the ^{13}C solid state NMR spectrum of the monomer DDSQ-ND-OCN after thermal treatment at each temperature. After thermal curing at 210 °C, the signal at 116.1 ppm for the O*CN units disappeared, consistent with the formation of triazine units. Although the signals for the aliphatic carbon nuclei at 41.2 and 50.3 ppm did not change after thermal curing at 210 °C, they disappeared after thermal treatment at 500 °C, consistent with the FTIR spectral analysis. Fig. 8(c) displays the ^{29}Si solid state NMR spectrum of the monomer DDSQ-ND-OCN after thermal treatment at each temperature. The signal of the SiOSi units appeared at −77.4 ppm and did not change after treatment at the different temperatures, suggesting that the inorganic DDSQ nanoparticles were not destroyed during high-temperature thermal treatment. In contrast, the signals for the Si–C units at −22.4 ppm disappeared after thermal treatment at 500 °C. Thus, the FTIR and NMR spectral data in Fig. 8 confirmed that cleavage of some of the C–H and C–C bonds of the ND groups occurred during thermal treatment at 500 °C (Scheme S2). As a result, the hexagonally packed cylindrical porous structure underwent collapse, resulting in a lower surface area for the mesoporous PCE/DDSQ framework.

To investigate the possible applications of these mesoporous PCE/DDSQ frameworks in energy storage, here we tested (Fig. 9) the electrochemical performance of the sample obtained after thermal treatment at 420 °C, because of its high surface area and well-defined hexagonal porous structure. To our best knowledge, this report is the first to discuss the electrochemical performance of such a material. We used a three-electrode cell and 1.0 M KCl as a green medium to provide a wide potential window for the CV curves (from −0.2 V to +1.0 V). The CV cycles revealed a major electric double layer capacitor (EDLC) throughout the range from 0.0 to 1.0 V and a minor pseudocapacitance (PC) within the range from −0.25 to 0.0 V [Fig. 9(a)]. This type of hybrid capacitor arose because of the chemical structure of the mesoporous PCE/DDSQ framework. This hybrid capacitor displayed a specific capacitance of 20 F g^{-1} at 5 mV s^{-1} [Fig. 9(b)]. This performance is comparable with that of some carbon materials performances-for example, some intercalated graphite derivatives that have an achieved specific capacitances of 5 F g^{-1} at 5 mV s^{-1}. We also observed efficient symmetrical charge/discharge performances at various tested currents (1–8 μA). These values were measured using a tested cell having dimensions of 0.5 × 0.5 cm^2 [Fig. 9(c)]. Moreover, Fig. 9(d) reveals an outstanding efficient cycling ability at 13 μA over 4000 cycles, with an excellent average capacitance retention of 95% with 100% columbic efficiencies, relative to the performance of other non-carbonized materials having a similar surface area.[44–50]

4. Conclusions

We have synthesized the monomer DDSQ-ND-OCN possessing high thermal stability after thermal polymerization treatment, the char yield increased from 68 to 81 wt% because of high thermal stability of the inorganic DDSQ nanoparticles and the formation of triazine units that increased the crosslinking density. In addition, the inorganic DDSQ nanoparticles were dispersed in PCE matrix homogeneously, as confirmed from SEM and TEM analyses revealing a hexagonally packed cylindrical porous structure; this porous structure collapsed, however, after thermal treatment at 500 °C, due to cleavage of some of the C–H and C–C bonds of the ND units. Most interestingly, this mesoporous PCE/DDSQ framework exhibited good electrochemical properties, and outstandingly efficient cycling ability at 13 μA over 4000 cycles, with an

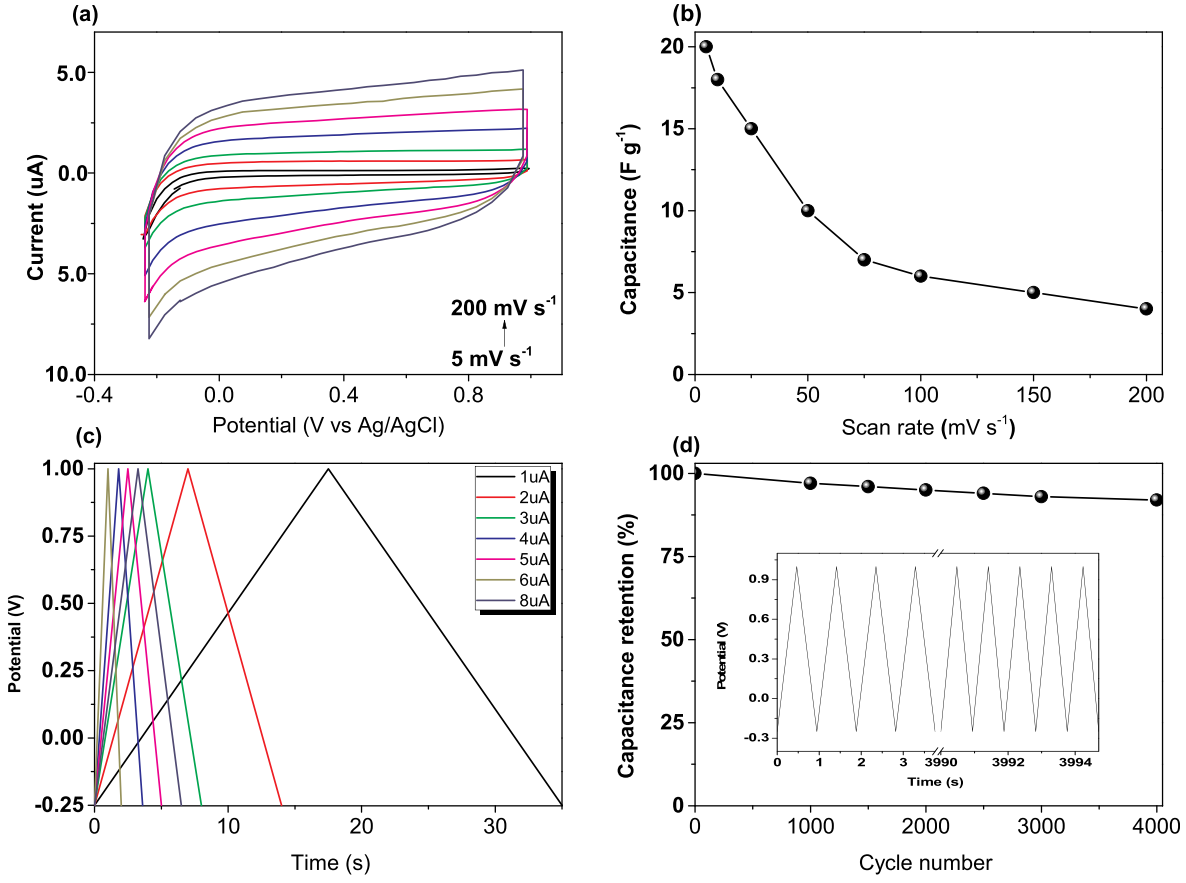

Fig. 9. Electrochemical performance of the mesoporous PCE/DDSQ framework: (a) CV traces recorded at scan rates from 5 to 200 mV s^{-1}; (b) capacitance plotted with respect to scan rate; (c) CD traces recorded at various current ranges; (d) capacitance retention at 13 μA over 4000 cycles (average retention: 95%).

excellent average capacitance retention of 95% with 100% columbic efficiencies, relative to that of other non-carbonized materials having a similar surface area.

Declaration of competing interest

The authors declare that they have no known competing financial interests or personal relationships that could have appeared to influence the work reported in this paper.

Acknowledgment

This study was supported financially by the Ministry of Science and Technology, Taiwan, under contracts MOST 106-2221-E-110-067-MY3 and 108-2221-E-110-014-MY3.

Appendix A. Supplementary data

Supplementary data to this article can be found online at https://doi.org/10.1016/j.polymer.2019.121940.

References

[1] T. Fang, D.A. shimp, Polycyanate esters: science and applications, Prog. Polym. Sci. 20 (1995) 61–118.
[2] S. Ohashi, J. Kilbane, T. Heyi, H. Ishida, Synthesis and characterization of cyanate ester functional benzoxazine and its polymer, Macromolecules 48 (2015) 8412–8417.
[3] X. Li, Y. Gu, The co-curing process of a benzoxazine-cyanate system and the thermal properties of the copolymers, Polym. Chem. 2 (2011) 2778–2781.
[4] Y.E. Xu, C.S.P. Sung, UV, luminescence, and FTIR characterization of cure reaction in bisphenol A dicyanate ester resin, Macromolecules 35 (2002) 9044–9048.
[5] A. Zegaoui, M. Derradji, A. Medjahed, A.Q. Dayo, W. Dong, W.B. Liu, W.A. Cai, J. Wang, Y.G. Liu, Multifunctional polymer materials with enhanced mechanical, thermal and gamma radiation shielding properties from dicyanate ester of bisphenol-A/bisphenol-A based benzoxazine resin and short kevlar/basalt hybrid fibers, J. Polym. Res. 25 (2018) 250.
[6] J. Bauer, M. Bauer, J. Kinetic structural model for the network build-up during the reaction of cyanic acid esters with glycidyl ethers, Macromol. Sci. Part A-Chem. 27 (1990) 97–116.
[7] A.M. Gupta, C.W. Macosko, Characterization and modeling of rigid branched polycyanates, Macromolecules 26 (1993) 2455–2463.
[8] M.W. Wang, R.J. Jeng, C.H. Lin, Origin of the rapid trimerization of cyanate ester in a benzoxazine/cyanate ester blend, Macromolecules 48 (2015) 2417–2421.
[9] H. Yu, C. Shen, M. Tian, J. Qu, Z. Wang, Microporous cyanate resins: synthesis, porous structure, and correlations with gas and vapor adsorptions, Macromolecules 45 (2012) 5140–5150.
[10] S. Graetz, H. Komber, M. Bauer, B. Voit, A Diels-Alder reaction between cyanates and cyclopentadienone-derivatives- a new class of crosslinkable oligomers, Polym. Chem. 10 (2019) 698–704.
[11] W.C. Li, W. Haung, Y. Kang, Y. Gong, Y. Ying, J. Yu, J.W. Zheng, L. Qiao, S.L. Che, Fabrication and investigations of G-POSS/cyanate ester resin composites reinforced by silane-treated silica fibers, Compos. Sci. Technol. 173 (2019) 7–14.
[12] D.Q. Peng, W. Qin, X.H. Wu, Improvement of the atomic oxygen resistance of carbon fiber reinforced cyanate ester composites modified by POSS-graphene-TiO_2, Polym. Degrad. Stab. 133 (2016) 211–218.
[13] X.B. Zhang, L. Yuan, Q.B. Guan, G.Z. Liang, A.J. Gu, Reatly improving energy storage density and reducing dielectric loss of carbon nanotube/cyanate ester composites through building a unique tri-layered structure with mica paper, J. Mater. Chem. A 5 (2017) 21909–21918.
[14] M. Venkatesh, S. Guothaman, S.O. Kanemoto, M.S. Lakeshim, I. Hamerton, Development of epoxy-cyanate ester-clay nanocomposites offering enhanced thermally stability, J. Appl. Polym. Sci. 136 (2019) 47754.
[15] W. Yuan, J.L. Feng, Z. Judeh, J. Dai, M.B. Chan-Park, Use of polyimide-graft-bisphenol a diglyceryl acrylate as a reactive noncovalent dispersant of single-walled carbon nanotubes for reinforcement of cyanate ester/epoxy composite, Chem. Mater. 22 (2010) 6542–6554.
[16] F. Ren, D.P. Song, Z. Li, L.C. Jia, Y.C. Zhao, D.X. Yan, P.G. Ren, Synergistic effect of graphene nanosheets and carbonyl iron-nickel alloy hybrid filler on electromagnetic interference shielding and thermal conductivity of cyanate ester composites, J. Mater. Chem. C 6 (2018) 1476–1486.
[17] S.W. Kuo, F.C. Chang, POSS related polymer nanocomposites, Prog. Polym. Sci. 36 (2011) 1649–1696.
[18] W. Zhang, S. Zhang, Q. Guo, X.L. Lu, Y.C. Liu, J.L. Mao, C. Wesdemiotis, T. Li, Y. W. Li, S.Z.D. Cheng, Multilevel manipulation of supramolecular structures of giant molecules via macromolecular composition and sequence, ACS Macro Lett. 7 (2018) 635–640.
[19] K.W. Huang, L.W. Tsai, S.W. Kuo, Influence of octakis-functionalized polyhedral oligomeric silsesquioxanes on the physical properties of their polymer nanocomposites, Polymer 50 (2009) 4876–4887.
[20] D. Han, T.J. Wen, G. Han, Y.Y. Deng, Y. Deng, Q. Zhang, Q. Fu, Synthesis of Janus POSS star polymer and exploring its compatibilization behavior for PLLA/PCL polymer blends, Polymer 136 (2018) 84–91.
[21] W.H. Hu, K.W. Huang, C.W. Chiou, S.W. Kuo, Complementary multiple hydrogen bonding interactions induce the self-assembly of supramolecular structures from heteronucleobase-functionalized benzoxazine and polyhedral oligomeric silsesquioxane nanoparticles, Macromolecules 45 (2012) 9020–9028.
[22] C.W. Chiou, Y.C. Lin, T. Hayakawa, S.W. Kuo, Hydrogen bond interactions mediate hierarchical self-assembly of POSS-containing block copolymers blended with phenolic resin, Macromolecules 47 (2014) 8709–8721.
[23] M.J. Huang, K. Yue, J.H. Huang, C. Liu, Z. Zhou, J. Wang, K. Wu, W.P. Shan, A. C. Shi, S.Z.D. Cheng, Highly asymmetric phase behaviors of polyhedral oligomeric silsesquioxane-based multiheaded giant surfactants, ACS Nano 12 (2018) 1868–1877.
[24] M.G. Mohamed, K.C. Hsu, J.L. Hong, S.W. Kuo, Unexpected fluorescence from maleimide-containing polyhedral oligomeric silsesquioxanes: nanoparticle and sequence distribution analyses of polystyrene-based alternating copolymer, Polym. Chem. 7 (2016) 135–145.
[25] C.F. Huang, S.W. Kuo, F.J. Lin, W.J. Huang, C.F. Wang, W.Y. Chen, F.C. Chang, Influence of PMMA-chain-end tethered polyhedral oligomeric silsesquioxanes (POSS) on the miscibility and specific interaction with phenolic blends, Macromolecules 39 (2006) 300–308.
[26] M.J. Huang, C.H. Hsu, J. Wang, S. Mei, X.H. Dong, Y.W. Li, M.X. Li, H. Liu, W. Zhang, T.Z. Aida, W.B. Zhang, K. Yue, S.Z.D. Cheng, Selective assemblies of giant tetrahedra via precisely controlled positional interactions, Science 338 (2015) 424–428.
[27] S.W. Kuo, Building blocks precisely from polyhedral oligomeric silsesquioxane nanoparticles, ACS Cent. Sci. 2 (2016) 62–64.
[28] G.M. Mohamed, S.W. Kuo, Polybenzoxazine/polyhedral oligomeric silsesquioxane (POSS) nanocomposites, Polymers 8 (2016) 225.
[29] T. Xu, Y. Cao, J. Xie, Q. Li, X.M. Chen, S.W. Kuo, L.Z. Dai, Mixed micelles from synergistic self-assembly of hybrid copolymers with charge difference electrostatic interaction induced Re-organization of micelles from hybrid copolymers, J. Mater. Res. 31 (2016) 2046–2057.
[30] S. Koutsoumpis, J. Ozimek, K.N. Raftopoulos, E. Hebda, P. Klonos, C.M. Papadakis, K. Pielichowski, P. Pissis, Polyurethanes with POSS pendent on flexible hard segments: morphology and glass transition, Polymer 147 (2018) 225–236.
[31] Z.S. Ge, D. Wang, Y.M. Zhou, H.W. Liu, S.Y. Liu, Synthesis of organic/inorganic hybrid quatrefoil-shaped star-cyclic polymer containing a polyhedral oligomeric silsesquioxane core, Macromolecules 42 (2009) 2903–2910.
[32] H.Y. Xu, B.H. Yang, J.F. Wang, S.Y. Guang, C. Li, Preparation, thermal properties, and T-g increase mechanism of poly(acetoxystyrene-co-octavinyl- polyhedral oligomeric silsesquioxane) hybrid nanocomposites, Macromolecules 38 (2005) 10455–10460.
[33] K. Zhang, Q. Zhuang, X. Liu, G. Yang, R. Cai, Z. Han, A new benzoxazine containing benzoxazole-functionalized polyhedral oligomeric silsesquioxane and the corresponding polybenzoxazine nanocomposites, Macromolecules 46 (2013) 2696–2704.
[34] Y.T. Liao, Y.C. Lin, S.W. Kuo, Highly thermally stable, transparent, and flexible polybenzoxazine nanocomposites by combination of double-decker-shaped polyhedral silsesquioxanes and polydimethylsiloxane, Macromolecules 50 (2017) 5739–5747.
[35] W.C. Chen, S.W. Kuo, Ortho-imide and allyl groups effect on highly thermal stable polybenzoxazine/double-decker–shaped polyhedral silsesquioxanes (DDSQ) nanocomposites, Macromolecules 51 (2018) 9602–9612.
[36] G.M. Mohamed, S.W. Kuo, Functional polyimide/polyhedral oligomeric silsesquioxane nanocomposites, Polymers 11 (2019) 26.
[37] G.M. Mohamed, S.W. Kuo, Functional silica and carbon nanocomposites based on polybenzoxazines, Macromol. Chem. Phys. 220 (2019) 1800306.
[38] S. Wu, T. Hayakawa, R. Kikuchi, S.J. Grunzinger, M. Kakimoto, Synthesis and characterization of semiaromatic polyimides containing POSS in main chain derived from double-decker-shaped silsesquioxane, Macromolecules 40 (2007) 5698–5705.
[39] S. Wu, T. Hayakawa, M. Kakimoto, H. Oikawa, Synthesis and characterization of organosoluble aromatic polyimides containing POSS in main chain derived from double-decker-shaped silsesquioxane, Macromolecules 41 (2008) 3481–3487.
[40] N. Liu, L. Li, L. Wang, S. Zheng, Organic-inorganic polybenzoxazine copolymers with double decker silsesquioxanes in the main chains: synthesis and thermally activated ring-opening polymerization behavior, Polymer 109 (2017) 254–265.
[41] C. Zhang, N. Liu, L. Li, L. Wang, S. Zheng, Polybenzoxazine nanocomposites containing 3,13-Diglycidyl double-decker silsesquioxane, Polym. Compos. 38 (2017) 827–836.
[42] P. Bartolomeo, J.F. Chailan, J.L. Vernet, Curing of cyanate ester resin: a novel approach based on FTIR spectroscopy and comparison with other techniques, Eur. Polym. J. 37 (2001) 659–670.
[43] J.Y. Wu, M.G. Mohamed, S.W. Kuo, Directly synthesized nitrogen-doped microporous carbons from polybenzoxazine resins for carbon dioxide capture, Polym. Chem. 8 (2017) 5481–5489.